JOURNAL OF COMPUTATIONAL PHYSICS 111, 183–193 (1994)

Numerical Simulation of Nonisothermal Capillary Interfaces

C. CHEN AND J. M. FLORYAN

Department of Mechanical Engineering, The University of Western Ontario, London, Ontario N6A 5B9, Canada

Received July 24, 1992; revised August 9, 1993

An effective algorithm for analysis of nonisothermal capillary interfaces has been developed. The algorithm is based on a coordinate transformation method. The unknown physical domain is mapped onto a rectangular computational domain, with the explicit form of the mapping function not being known. The field variables and the mapping function are determined simultaneously using Picard-type iteration. The algorithm is based on the second-order finite difference discretization and delivers the second-order accuracy, even for very large interfacial distortions. © 1994 Academic Press, Inc.

I. INTRODUCTION

Zero gravity environment offers potential for development of novel material processing techniques. The effectiveness of many of these techniques depends on the ability to control transport processes taking place in the liquid phase. Thermocapillary effect, which is gravity independent, is expected to play a dominant role. Understanding of the dynamics of nonisothermal interfaces and how it changes as a function of geometrical constraints is, therefore, imperative. The main objective of this work is to develop an algorithm capable of accurate prediction of the response of an interface to external temperature fields.

Variation of surface tension as a function of temperature induces tangential force along the interface which, in turn, generates motion in the adjacent phases. The final shape of the interface results from an interaction between the surface tension and the pressure and normal viscous stresses generated by the convection field. The actual form of the surface tension variations depends on the energy transport in the adjacent phases. Analysis of the topology of the interfaces requires, therefore, determination of the solutions of the moving boundary problems for the Navier–Stokes and energy equations. Since it is an interplay between the surface tension gradients and the viscous stresses that determines the dynamics of the system, these two effects have to be modelled very accurately.

Algorithms for moving boundary problems for the Navier–Stokes equations have been recently reviewed by Floryan and Rasmussen [1]. These algorithms can be based on Eulerian, Lagrangian, and mixed formulations. Our present interest is in steady problems which are best dealt with using Eulerian formalism. Moving interface can be described either in terms of fixed grids, or in terms of adaptive grids, or by applying analytical mapping techniques. In the first approach, interface travels through a fixed grid and this leads to difficulties in accurate determination of the location, orientation, and curvature of the interface between the grid points. The last two factors are crucial in our problem because they affect modelling of normal viscous stress and surface tension effects at the interface. In the second approach, grid is regenerated numerically so that one of the grid lines always overlaps with the interface. Interfacial effects can be accurately modelled, but the cost of calculations may be very high due to repetitive numerical coordinate generations. It is also difficult to estimate the overall error due to the combination of errors originating from the numerically generated grid and from the discretized field equations. In the third approach, grid generation is replaced by an analytical mapping technique that transfers the problem from an irregular physical domain into a regular computational domain. The mapping function is unknown and has to be determined as a part of the solution procedure. Since this approach is computationally more efficient and accurate, it has been selected as the base of the present work.

Shokoohi and Elrod [2, 3] used a coordinate mapping technique in the analysis of capillary break-up of a cylindrical jet. A special discretization technique was used which resulted in high consumption of computing resources. Strani and Piva [4] used a similar mapping in the analysis of thermocapillary convection. They coupled primitive variables formulation with the MAC discretization procedure. It is difficult to assess the accuracy of their solution, especially for large deformations, since only the results for grids $10 * 10$ are given. Chen *et al.* [5] considered the same problem, but used numerically generated boundary fitted coordinates. The issue of the effective accuracy of the algorithm was not discussed.

In the present work, we focus our attention on the

0021-9991/94 $6.00

standard second-order finite difference discretization technique and apply them in the analysis of the behaviour of non-isothermal interface and the adjacent phase. Geometry of the solution domain is regularized using a coordinate transformation method. A domain perturbation solution is developed to provide a test and motivation for the general algorithm. Streamfunction-vorticity formulation is used in the actual calculations. The paper is organized as follows: Section II discusses the model problem. Section III describes the domain perturbation solution. Section IV describes a direct algorithm for large interfacial deformations. Finally, Section V provides a short summary of the main conclusions.

II. THE MODEL PROBLEM

Consider a rectangular cavity as shown in Fig. 1. The upper surface, described by $y=h(x)$, is a free surface bounded by a passive gas of negligible density and viscosity. Temperature distribution in the gas $T=T_g(x)$ is assumed to be known. Motion of the liquid is induced by variations of surface tension arising due to thermocapillary effect. Shape of the interface results from the balance of forces at the interface. The contributing factors are the local value of the surface tension (which depends on the local temperature resulting from the overall energy transport) and the pressure and viscous stresses associated with the convection field. Physical motivation and the relevant scaling are described in Ref. [6].

In the absence of body forces, the steady two-dimensional motion of the liquid is governed by the equations

$$u_x + v_y = 0 \tag{1a}$$

$$\mathrm{Re}(uu_x + vu_y) = -p_x + u_{xx} + u_{yy} \tag{1b}$$

$$\mathrm{Re}(uv_x + vv_y) = -p_y + v_{xx} + v_{yy} \tag{1c}$$

$$\mathrm{Ma}(uT_x + vT_y) = T_{xx} + T_{yy} \tag{1d}$$

where u and v are respectively x and y components of the velocity vector, p is the pressure, T is the temperature of the liquid, Re and Ma are respectively Reynolds and Marangoni numbers. These equations are subject to the following boundary conditions:

$$x=-\tfrac{1}{2}L: \qquad u=v=0, \quad T=T_L \tag{2a}$$

$$x=\tfrac{1}{2}L: \qquad u=v=0, \quad T=T_R \tag{2b}$$

$$y=0: \qquad u=u=T_y=0 \tag{2c}$$

$$y=h(x): \qquad v=uh_x \tag{2d}$$

$$-p+2(1+h_x^2)^{-1}\,[h_x^2u_x+v_y-h_x(v_x+u_y)] = C^{-1}h_{xx}(1-CT)(1+h_x^2)^{-3/2} \tag{2e}$$

$$(1-h_x^2)(u_y+v_x)+2h_x(v_y-u_x) = -(1+h_x^2)^{1/2}\,(T_x+h_xT_y) \tag{2f}$$

$$(1+h_x^2)^{-1/2}\,(T_y-h_xT_x)+\mathrm{Bi}[T-T_g(x)]=0. \tag{2g}$$

In the above, C denotes the capillary number and Bi stands for the Biot number. Left and right walls of the cavity are assumed to be isothermal and the bottom is assumed to be insulated. Equation (2d) describes kinematic condition at the interface, (2e) and (2f) describe the balance of normal and tangential forces at the interface, respectively, and (2g) specifies a general heat transfer condition at the interface. Thermal boundary conditions (2a) and (2b), and the temperature distribution in the gas phase $T_g(x)$ in (2g) must satisfy the consistence conditions at the upper corners. The deformed interface must satisfy the mass conservation constraint

$$\int_{-1/2L}^{1/2L} h(x)\,dx = V. \tag{3}$$

The problem is closed by specifying the type of contact made by the interface at the end walls. Two cases will be considered:

(i) fixed contact points,

$$h(-\tfrac{1}{2}L)=D_L, \qquad h(\tfrac{1}{2}L)=D_R; \tag{4a}$$

(ii) fixed contact angles (moving contact points),

$$h_x(-\tfrac{1}{2}L)=\tan\theta_L, \qquad h_x(\tfrac{1}{2}L)=-\tan\theta_R. \tag{4b}$$

The type of contact that may exist between the interface and the side wall leads to a qualitatively different response of the whole flow system (Section IV).

One may note that there are three boundary conditions given at the interface, and this permits writing a condition for determination of the unknown function $h(x)$, describing the location of the interface.

III. DOMAIN PERTURBATION SOLUTION

A. *Preliminaries*

The domain perturbation solution is based on the assumption that the shape of the interface can be accurately estimated without solving the whole problem. Then, the actual location of the interface is described as a small perturbation around the initial estimate. The complete moving boundary problem (1)–(4) splits into a convection problem with the known location of the interface (fixed boundary problem) followed by evaluation of the (small) deformation of the interface. It remains to settle which boundary condition at the interface should be used for evaluation of its deformation.

B. *Small Deformation Theory*

We consider solution of the problem (1)–(4) in the asymptotic limit of $C \to 0$, which corresponds to the case of small surface tension variations as compared to mean surface tension. The interface is dominated by capillary forces with the thermocapillary effect producing only small distortions (see Ref. [6] for a discussion).

The flow quantities are represented as

$$q = q_0 + Cq_1 + O(C^2) \tag{5a}$$

$$p = C^{-1}p_s + p_0 + Cp_1 + O(C^2), \tag{5b}$$

where q stands for u, v, T, and h. Substitution of (5) into (1)–(4) results in:

Problem $O(C^{-1})$,

$$p_{sx} = 0, \qquad p_{sy} = 0 \tag{6a}$$

$$-p_s = h_{0xx}(1 + h_{0x}^2)^{-3/2} \tag{6b}$$

$$\int_{-1/2L}^{1/2L} h_0\, dx = V \tag{6c}$$

$$h_0(-\tfrac{1}{2}L) = D_L \quad \text{or} \quad h_{0x}(-\tfrac{1}{2}L) = \tan\theta_L \tag{6d}$$

$$h_0(\tfrac{1}{2}L) = D_R \quad \text{or} \quad h_{0x}(\tfrac{1}{2}L) = -\tan\theta_R \tag{6e}$$

Problem $O(C^0)$: *Flow problem,*

$$u_{0x} + v_{0y} = 0 \tag{7a}$$

$$\mathrm{Re}(u_0 u_{0x} + v_0 u_{0y}) = -p_{0x} + u_{0xx} + u_{0yy} \tag{7b}$$

$$\mathrm{Re}(u_0 v_{0x} + v_0 v_{0y}) = -p_{0y} + v_{0xx} + v_{0yy} \tag{7c}$$

$$\mathrm{Ma}(u_0 T_{0x} + v_0 T_{0y}) = T_{0xx} + T_{0yy} \tag{7d}$$

$$x = -\tfrac{1}{2}L: \quad u_0 = v_0 = 0, \quad T_0 = T_L \tag{7e}$$

$$x = \tfrac{1}{2}L: \quad u_0 = v_0 = 0, \quad T_0 = T_R \tag{7f}$$

$$y = 0: \quad u_0 = v_0 = T_{0y} = 0 \tag{7g}$$

$$y = h_0(x): \quad v_0 = u_0 h_{0x} \tag{7h}$$

$$(1 - h_{0x}^2)(u_{0y} + v_{0x}) + 2h_{0x}(v_{0y} - u_{0x}) = -(1 + h_{0x}^2)^{1/2}(T_{0x} + h_{0x}T_{0y}) \tag{7i}$$

$$(1 + h_{0x}^2)^{-1/2}(T_{0y} - h_{0x}T_{0x}) + \mathrm{Bi}(T_0 - T_g) = 0 \tag{7j}$$

Deformation problem,

$$y = h_0(x): \quad -p_0 + 2(1 + h_{0x}^2)^{-1} \times [h_{0x}^2 u_{0x} + v_{0y} - h_{0x}(v_{0x} + u_{0y})] = \{h_{1xx} - h_{0xx}[T_0 + 3(1 + h_{0x}^2)^{-1} h_{0x}h_{1x}]\} \times (1 + h_{0x}^2)^{-3/2} \tag{8a}$$

$$\int_{-1/2L}^{1/2L} h_1\, dx = 0 \tag{8b}$$

$$h_1(-\tfrac{1}{2}L) = 0 \quad \text{or} \quad h_{1x}(-\tfrac{1}{2}L) = 0 \tag{8c}$$

$$h_1(+\tfrac{1}{2}L) = 0 \quad \text{or} \quad h_{1x}(\tfrac{1}{2}L) = 0. \tag{8d}$$

Leading-order problem (Eq. (6)) describes the initial approximation of the shape of the interface. It consists of the Young–Laplace equation (6b) (describing isothermal capillary surfaces) whose solutions are given by either a straight line or by an element of a circle. The orientation of the straight line and the radius of curvature and location of the centre of curvature for a particular arc element are determined by the mass constraint (6c) and the contact conditions (6d)–(6e). One many note that (6c) and (6d)–(6e) have to satisfy the consistency conditions for a solution to exist.

Equations (7a)–(7j) describe the flow problem for the known location $h_0(x)$ of the interface. The problem is closed without including the normal stress boundary condition at the interface.

Equations (8a)–(8d) describe deformation $h_1(x)$ of the interface on the basis of the normal stress boundary condition (8a) subject to volumetric constraint (8b) and contact conditions (8c)–(8d).

C. *Coordinate Transformation Method*

Flow problem (7) has to be solved numerically on an irregular solution domain (as defined by $h_0(x)$). After application of the transformation,

$$\xi = x, \qquad \eta = y/h_0(x), \tag{9}$$

the domain assumes a rectangular shape in the (ξ, η) plane (Fig. 1) and this permits the application of the standard finite difference discretizations. Field equations (7a)–(7d) are expressed in terms of streamfunction (ψ)–vorticity (ω) formulation in the form

$$\nabla^2\psi = -\omega \tag{10a}$$

$$\nabla^2\omega = \mathrm{Re}\, h_0^{-1}(\psi_\eta \omega_\xi - \psi_\xi \omega_\eta) \tag{10b}$$

$$\nabla^2 T_0 = \mathrm{Ma}\, h_0^{-1}(\psi_\eta T_{0\xi} - \psi_\xi T_{0\eta}), \tag{10c}$$

where

$$u_0 = \psi_y, \qquad v_0 = -\psi_x, \qquad \omega = -u_{0y} + v_{0x},$$

$$\nabla^2 = \partial^2/\partial\xi^2 - 2\eta h_{0\xi} h_0^{-1}\partial^2/\partial\xi\,\partial\eta + (\eta^2 h_{0\xi}^2 + 1)\, h_0^{-2}\partial^2/\partial\eta^2 + (2h_{0\xi}^2 - h_0 h_{0\xi\xi})\, \eta h_0^{-2}\partial/\partial\eta. \tag{10d}$$

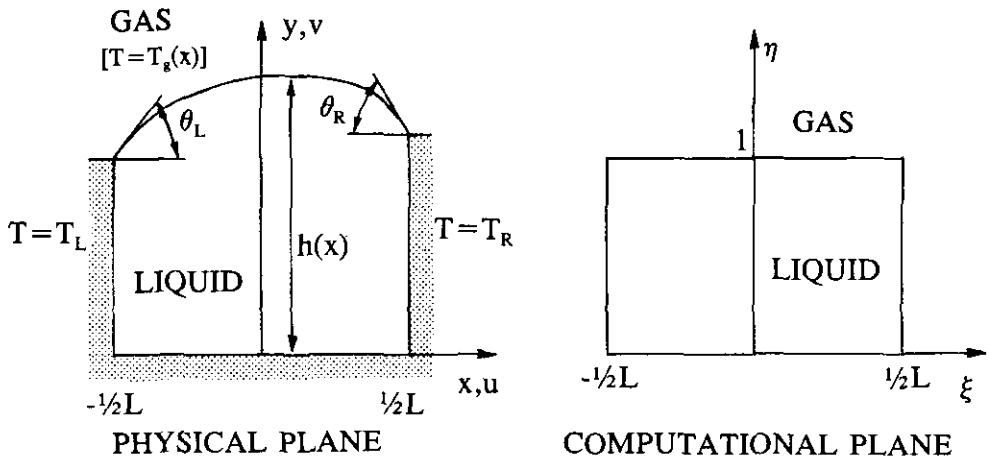

FIG. 1. Sketch of the model problem.

The boundary conditions transform to

$$\xi = -\tfrac{1}{2}L: \quad \psi = \psi_\xi = 0, \quad T_0 = T_L \tag{10e}$$

$$\xi = \tfrac{1}{2}L: \quad \psi = \psi_\xi = 0, \quad T_0 = T_R \tag{10f}$$

$$\eta = 0: \quad \psi = \psi_\eta = 0, \quad T_{0\eta} = 0 \tag{10g}$$

$$\eta = 1: \quad \psi = 0 \tag{10h}$$

$$(1+h_{0\xi}^2)^2 h_0^{-2}\psi_{\eta\eta} - 2h_{0\xi}(1+h_{0\xi}^2) h_0^{-1}\psi_{\xi\eta} + [(1-h_{0\xi}^2) h_0 h_{0\xi\xi} + (1+h_{0\xi}^2) 2h_{0\xi}^2] h_0^{-2}\psi_\eta = -(1+h_{0\xi}^2)^{1/2} T_{0\xi} \tag{10i}$$

$$(1+h_{0\xi}^2)^{1/2} h_0^{-1} T_{0\eta} - h_{0\xi}(1+h_{0\xi}^2)^{-1/2} T_{0\xi} + \mathrm{Bi}(T_0 - T_g) = 0. \tag{10j}$$

D. *The Numerical Method*

A rectangular computational grid of size $\Delta\xi$, $\Delta\eta$ in the ξ, η directions is considered, with grid lines parallel to the ξ and η axes and such that the grid fits exactly the geometry of the computational domain, with the side and bottom walls and the interface as certain grid lines. Around a typical interior grid point (ξ_0, η_0) we adopt the convention that quantities at (ξ_0, η_0) and in the eight neighbouring points are denoted by subscripts 0, 1, ..., 8, as shown in Fig. 2. Then (10a)–(10b) are approximated by using central second-order differences in the usual manner, to give

$$-2(A_1+A_2)\psi_0 + A_1\psi_1 - A_3\psi_2 + (A_2+A_4)\psi_3 + A_3\psi_4 + A_1\psi_5 - A_3\psi_6 + (A_2-A_4)\psi_7 + A_3\psi_8 + \omega_0 = 0 \tag{11a}$$

$$-2(A_1+A_2)\omega_0 + [A_1 - \mathrm{Re}\, A_5(\psi_3-\psi_7)]\omega_1 - A_3\omega_2 + [A_2 + A_4 + \mathrm{Re}\, A_5(\psi_1-\psi_5)]\omega_3 + A_3\omega_4 + [A_1 + \mathrm{Re}\, A_5(\psi_3-\psi_7)]\omega_5 - A_3\omega_6 + [A_2 - A_4 - \mathrm{Re}\, A_5(\psi_1-\psi_5)]\omega_7 + A_3\omega_8 = 0, \tag{11b}$$

where

$$A_1 = \Delta\xi^{-2}, \qquad A_2 = (1+\eta^2 h_{0\xi}^2)(h_0\,\Delta\eta)^{-2},$$
$$A_3 = \eta h_{0\xi}(2h_0\,\Delta\xi\,\Delta\eta)^{-1}$$
$$A_4 = \eta(2h_{0\xi}^2 - h_0 h_{0\xi\xi})(2h_0^2\,\Delta\eta)^{-1},$$
$$A_5 = (4h_0\,\Delta\xi\,\Delta\eta)^{-1}.$$

The discretized energy equation has the same form as (11b) with ω replaced by T_0 and Re replaced by Ma.

The boundary conditions for (11) are given by (10e)–(10j). For (11a), the values of ψ are known at all the grid points on the solid walls and along the interface. For (11b), a boundary condition for ω is required at the grid points on the solid walls. Here, we use a second-order approximation for the side walls

$$\omega_b = (\psi_{i+1} - 8\psi_i)/(2\Delta^2), \tag{12a}$$

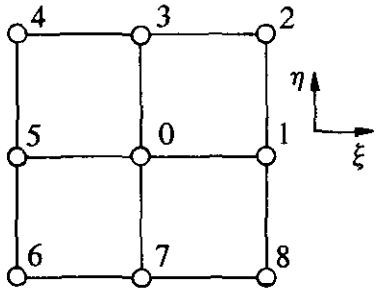

FIG. 2. Sketch of a typical computational molecule.

where subscript b refers to the wall values, subscript i refers to the internal grid point most immediate to b, subscript $i+1$ refers to the next grid point in the same direction, and Δ denotes the grid size. A similar formula for the bottom of the cavity has the form

$$\omega_b = \frac{\psi_{i+1} - 8\psi_i}{2\Delta^2 h_0^2}. \tag{12b}$$

The boundary condition at the interface is obtained by substituting (10i) into (10a), resulting in

$$\omega = \frac{(1+h_{0\xi}^2)^{1/2}\, T_{0\xi} h_0 + 2h_{0\xi\xi}\psi_\eta}{h_0(1+h_{0\xi}^2)}. \tag{13}$$

In the above, $T_{0\xi}$ is evaluated using standard central-difference approximation, and ψ_η is determined using one-sided difference approximation. Both, $T_{0\xi}$ and ψ_η have to be updated during the iteration process. For the energy equation, values of T_0 are known at the side walls. At the remaining two boundaries T_0 is determined from the discretized boundary conditions (10g) and (10j). All discretization formulas are second-order accurate.

The discretized equations were solved by the standard Gauss–Seidel relaxation procedure. The systematic iterative procedure between the various equations consisted of performing one complete Gauss–Seidel iteration of (11a), followed by a similar iteration of (11b) and then a complete iteration of the energy equation followed by a recalculation of the boundary values of ω and T_0. The iterations were performed until the convergence criteria,

$$|\omega^{(i+1)} - \omega^{(i)}| < \varepsilon, \qquad |\psi^{(i+1)} - \psi^{(i)}| < \varepsilon,$$
$$|T_0^{(i+1)} - T_0^{(i)}| < \varepsilon,$$
$$|\mathrm{Res}_1^{(i)}| < \varepsilon, \qquad |\mathrm{Res}_2^{(i)}| < \varepsilon, \qquad |\mathrm{Res}_3^{(i)}| < \varepsilon,$$

with $\varepsilon = 10^{-6}$ and i denoting the iteration number, were satisfied at all grid points. In the above, Res_1, Res_2, and Res_3 stand for the residua of the discretized equations (10a), (10b), and (10c), respectively. Those criteria were judged to be generally satisfactory; nevertheless certain cases were additionally checked by reducing the criteria to $\varepsilon = 10^{-9}$. Usually, it was most difficult to satisfy the criterion for Res_2. The relaxation factor used in the calculations varied from 1.0 for flat interfaces to 0.05 for very deformed interfaces. These factors had to be further reduced with increasing values of Re and Ma.

E. *Testing of Accuracy of the Numerical Solution of the Field Equations*

It is of primary importance to determine how the coordinate transformation (9) affects the accuracy of the algorithm, specifically for cases corresponding to large distortions of the interface. The algorithm is formally second-order accurate; i.e., the discretization error is $O(\Delta\xi^2, \Delta\eta^2)$. The actual accuracy is determined on the basis of calculations with different grid sizes and by observing the tendency of results as $\Delta\xi = \Delta\eta = \Delta$ is decreased.

Solutions were obtained for $\Delta = 1/20,\ 1/40,\ 1/80$. If one assumes that the discretization error is $\hat{C}\Delta^\alpha$, with $\hat{C}$ being a constant (this is true for a sufficiently small Δ), then the exponent α can be evaluated as

$$\alpha = \ln(\varepsilon_{40/80}/\varepsilon_{20/40})/\ln 2, \tag{14}$$

where

$$\varepsilon_{40/80} = \frac{1}{N}\left[\sum_{i=1}^{N} (S_{40}^i - S_{80}^i)^2\right]^{1/2},$$
$$\varepsilon_{20/40} = \frac{1}{N}\left[\sum_{i=1}^{N} (S_{20}^i - S_{40}^i)^2\right]^{1/2}.$$

In the above, S stands for a solution quantity, subscripts 20, 40, 80 refer to solutions obtained on grids $\frac{1}{20}$, $\frac{1}{40}$, $\frac{1}{80}$, respectively, and summation extends over all grid points that overlap on all three grids employed. If the algorithm behaves according to the theoretical predictions, then Eq. (14) should yield the theoretical value of $\alpha = 2$. Departures from this value can be used as a measure of the loss of accuracy of the algorithm.

All tests presented in Table I have been carried out on a square cavity with $\mathrm{Re} = \mathrm{Ma} = 30$. The first test deals with a reference case of an isothermal flow with a flat interface and shear stress condition (7i) replaced by a known velocity distribution $u = 16 * (0.5 - x)^2 (0.5 + x)^2$. This particular velocity distribution has been selected in order to reduce singularities at the upper corners. In the second test, we returned to the original boundary conditions and specified $\mathrm{Bi} = \infty$ in the heat transfer boundary condition (7j), thus

TABLE I

Results of Grid Convergence Tests of the Algorithm Solving Field Equations with Various Degrees of Boundary Deformation (Section III.E)

Test	ψ	ω	T_0
1	2.18	1.76	Not calculated
2	1.84	2.08	1.99
3	1.57	2.44	1.86
4	1.33	1.67	1.69
5	1.62	1.39	1.56
6	1.48	0.82	1.44
7	1.12	0.81	1.28

Note. Displayed results are for $\mathrm{Re} = \mathrm{Ma} = 30$, $L = 1$ (see text for further details).

decoupling the energy transport equation. Shear stress at the interface was specified by assuming that $T_{0x} = T_{0\xi} \approx (0.5-x)^2 (0.5+x)^2$ in (7i). The third test was a repetition of the second one with $\mathrm{Bi} = 1$ and $T_{gx} = T_{g\xi} \approx (0.5-x)^2 (0.5+x)^2$. In the fourth test, we changed the shape of the interface to the form $h_0(x) = 1 + A\cos(2\pi x)$ with $A = 0.3$. In the fifth, sixth, and seventh tests, we increased A to 0.5, 0.6, and 0.7, respectively. Topology of the flow field for $A = 0.5$ is shown in Fig. 3.

The first test shows that the algorithm under standard conditions approximately reproduces the second-order accuracy. This test also illustrates that while the theoretical value of the exponent α is two, the actual value could be somewhat different due to assumptions involved in Eq. (14). The second test shows that the same accuracy is maintained with the shear stress boundary condition. The third test shows reduction in the accuracy due to singularity in the temperature field at the upper corners. The fourth and fifth tests show that the same accuracy is maintained by deforming the interface by up to 50%. Tests six and seven show a decrease of the accuracy associated with high deformations of the interface. While tests 2–7 should be viewed only as qualitative (they are somewhat contaminated by the presence of singularity in the temperature field), they demonstrate nevertheless that the algorithm maintains fairly high accuracy even for deformations reaching 50% of the depth of the cavity. Further increase of the deformation reduces the algorithm to first-order accurate.

F. *Numerical Solution of the Deformation Problem*

Deformation equation (8a) is rewritten with the help of (9) and (10d) as

$$h_{1\xi\xi} + H(\xi)\, h_{1\xi} = M(\xi) + KN(\xi), \tag{15}$$

where

$$H(\xi) = -3h_{0\xi}h_{0\xi\xi}(1+h_{0\xi}^2)^{-1}$$

$$M(\xi) = -p_0(1+h_{0\xi}^2)^{3/2} + 2(1+h_{0\xi}^2)^{1/2} \times [-(1+h_{0\xi}^2)\, h_0^{-1}\psi_{\xi\eta} + h_{0\xi}h_0^{-2} \times (h_{0\xi}^2 - h_{0\xi\xi}h_0 + 1)\psi_\eta] + h_{0\xi\xi}T_0$$

$$N(\xi) = -(1+h_{0\xi}^2)^{3/2}$$

with p_0, T_0, $\psi_{\xi\eta}$, ψ_η evaluated at $\eta = 1$. Here, p_0 stands for the normalized pressure satisfying condition $p_0(0, 1) = 0$ and K denotes an unknown additive constant that can be present in the pressure field. Pressure p_0 at the interface is evaluated from (7b)–(7c) on the basis of the known solution of (10), e.g.,

$$p_{0\xi} = h_{0\xi}\omega_\xi - (1+h_{0\xi}^2)\, h_0^{-1}\omega_\eta - \mathrm{Re}\, h_0^{-2}\psi_\eta \times [(1+h_{0\xi}^2)\,\psi_{\xi\eta} + h_{0\xi}h_0^{-1}(h_{0\xi\xi}h_0 - h_{0\xi}^2 - 1)\,\psi_\eta]. \tag{16}$$

The above expression is integrated using the trapezoidal rule in the $\pm\xi$ directions beginning at $\xi = 0$. A mixed derivative of the streamfunction at the interface is evaluated according to the formula

$$\psi_{\xi\eta} = [3(\psi_2 - \psi_4) - 4(\psi_1 - \psi_5) + \psi_8 - \psi_6]/(4\Delta\xi\,\Delta\eta) + O(\Delta\xi^2) + O(\Delta\eta^2),$$

where the subscripts refer to the points shown schematically in Fig. 2, with the points 2, 3, and 4 located on the interface. Other mean flow quantities are evaluated using standard one-sided or central second-order finite difference approximations.

The deformation equation (15) is linear, thus its solution consists of a superposition of two linearly independent solutions of the homogeneous problem and a particular solution of the inhomogeneous problem. Two boundary conditions (8c)–(8d) and volumetric constraint condition (8b) provide the required three conditions for the determination of the two constants of superposition and the pressure constant K.

Numerical solution of (15), subject to volumetric constraint (8b) and boundary conditions (8c)–(8d) begins with the discretization of (15) using standard central difference formulas and approximation of (8b) using the trapezoidal rule. The grid already used for the determination of the flow field is used in both cases. If the values of h_i at the grid points are denoted by $\hat{h}_i$, $i = 1, \ldots, N$, with $i = 1$ (N), corresponding to the left (right) contact point, the system of the linear algebraic equations for $\hat{h}_i$ and K in the case of fixed contact point conditions has the form

$$\begin{bmatrix} B_2 & C_2 & \cdot & \cdot & \cdot & & & & & -N_2 \\ A_3 & B_3 & C_3 & \cdot & \cdot & & & & & -N_3 \\ \cdot & A_4 & B_4 & C_4 & \cdot & & & & & -N_4 \\ & & & & \vdots & & & & & \vdots \\ & & & & \cdot & A_{N-3} & B_{N-3} & C_{N-3} & & -N_{N-3} \\ & & & & \cdot & \cdot & A_{N-2} & B_{N-2} & C_{N-2} & -N_{N-2} \\ & & & & \cdot & \cdot & \cdot & A_{N-1} & B_{N-1} & -N_{N-1} \\ D_2 & D_3 & D_4 & D_5 & \cdot & D_{N-4} & D_{N-3} & D_{N-2} & D_{N-1} & \end{bmatrix} \times \begin{Bmatrix} \hat{h}_2 \\ \hat{h}_3 \\ \hat{h}_4 \\ \vdots \\ \hat{h}_{N-3} \\ \hat{h}_{N-2} \\ \hat{h}_{N-1} \\ K \end{Bmatrix} = \begin{Bmatrix} M_2 \\ M_3 \\ M_4 \\ \vdots \\ M_{N-3} \\ M_{N-2} \\ M_{N-1} \\ W \end{Bmatrix}, \tag{17}$$

where only the nonzero elements are shown. In the above,

$$A_i = \Delta\xi^{-2} - \tfrac{1}{2}\Delta\xi^{-1} H_i, \qquad B_i = -2\Delta\xi^{-2},$$
$$C_i = \Delta\xi^{-2} + \tfrac{1}{2}\Delta\xi^{-1} H_i, \qquad H_i = H(\hat{h}_i),$$
$$N_i = N(\hat{h}_i), \qquad D_i = \Delta\xi \qquad \text{for} \quad i = 2, ..., N-1,$$
$$M_i = M(\hat{h}_i) \qquad \text{for} \quad i = 3, ..., N-2,$$
$$M_2 = M(\hat{h}_2) - A_2\hat{h}, \qquad M_{N-1} = M(\hat{h}_{N-1}) - C_{N-1}\hat{h}_N,$$
$$W = V - \tfrac{1}{2}\Delta\xi\,(\hat{h}_1 + \hat{h}_N),$$

where the volumetric constraint V and the locations of the end points, $\hat{h}_1$, $\hat{h}_N$ are kept nonzero for generality purposes. A very efficient algorithm for the direct solution of (17) is described in Appendix A. Changing the fixed contact point conditions into fixed contact angle conditions leads to the approximation of the slope of the interface at the contact points in the form

$$\begin{aligned} h_{1\xi} &= (-3\hat{h}_1 + 4\hat{h}_2 - \hat{h}_3)/2\Delta\xi + O(\Delta\xi^2) = M_1, \\ \xi &= -\tfrac{1}{2}L, \\ h_{1\xi} &= (3\hat{h}_N - 4\hat{h}_{N-1} + \hat{h}_{N-2})/2\Delta\xi + O(\Delta\xi^2) = M_N, \\ \xi &= \tfrac{1}{2}L, \end{aligned} \tag{18}$$

and results in the matrix equation of the following structure:

$$\begin{bmatrix} B_1 & C_1 & G_1 & \cdot & \cdot & & & & & \cdot \\ A_2 & B_2 & C_2 & \cdot & \cdot & & & & & -N_2 \\ \cdot & A_3 & B_3 & C_3 & & & & & & -N_3 \\ & & & & \vdots & & & & & \vdots \\ & & & & \cdot & A_{N-2} & B_{N-2} & C_{N-2} & \cdot & -N_{N-2} \\ & & & & \cdot & \cdot & A_{N-1} & B_{N-1} & C_{N-1} & -N_{N-1} \\ & & & & \cdot & \cdot & G_N & A_N & B_N & \cdot \\ D_1 & D_2 & D_3 & D_4 & \cdot & D_{N-3} & D_{N-2} & D_{N-1} & D_N & \cdot \end{bmatrix}$$
$$\times \begin{Bmatrix} \hat{h}_1 \\ \hat{h}_2 \\ \hat{h}_3 \\ \vdots \\ \hat{h}_{N-2} \\ \hat{h}_{N-1} \\ \hat{h}_N \\ K \end{Bmatrix} = \begin{Bmatrix} M_1 \\ M_2 \\ M_3 \\ \vdots \\ M_{N-2} \\ M_{N-1} \\ M_N \\ V \end{Bmatrix}, \tag{19}$$

In the above,

$$-B_1 = B_N = \tfrac{3}{2}\Delta\xi^{-1}, \qquad C_1 = -A_N = 2\Delta\xi^{-1},$$
$$G_1 = -G_N = -\tfrac{1}{2}\Delta\xi^{-1}, \qquad D_1 = D_N = \tfrac{1}{2}\Delta\xi,$$
$$A_i = \Delta\xi^{-2} - \tfrac{1}{2}\Delta\xi^{-1} H_i, \qquad B_i = -2\Delta\xi^{-2},$$
$$C_i = \Delta\xi^{-2} + \tfrac{1}{2}\Delta\xi^{-1} H_i, \qquad D_i = \Delta\xi, \quad i = 2, ..., N-1,$$

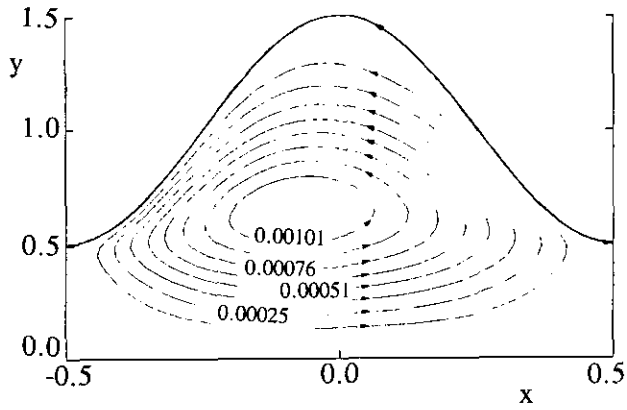

FIG. 3. Flow pattern for interface described by equation $h_0 = 1 + 0.5\cos(2\pi x)$ (Section III.E).

and with H_i, N_i, M_i having the same meaning as before, with the exception of $M_2 = M(\hat{h}_2)$, $M_{N-1} = M(\hat{h}_{N-1})$ and M_1, M_N defined by (18). A very efficient algorithm for the direct solution of (19) is described in Appendix B.

Three initial approximations of the shape $h_0(x)$ of the interface were used for the testing purposes. In the first test $h_0(x) = 1$ (flat interface), in the second one, $h_0(x) = 1.1 - L^2/1.6 + [(L^2/1.6 + 0.1)^2 - (x - 0.5)^2]^{1/2}$ (interface bulging out, $h_{0\max} = 1.2$), and in the third one, $h_0(x) = 0.9 + L^2/1.6 - [(L^2/1.6 + 0.1)^2 - (x - 0.5)^2]^{1/2}$ (interface bulging in, $h_{0\min} = 0.8$). All these shapes correspond to solutions of the isothermal capillary problem (6). Calculations were carried out for $\mathrm{Re} = \mathrm{Ma} = 30$, $\mathrm{Bi} = 10^4$, $T_{gx} = T_{g\xi} = (0.5 - x)^2\,(0.5 + x)^2$ on grids $\Delta\xi = \Delta\eta = \Delta = \frac{1}{20}, \frac{1}{40}, \frac{1}{80}$ and the variations of errors as a function of the grid size were estimated according to the formula (14). Table II gives values of the exponent α for all flow quantities entering the deformation equation (e.g., ψ_η, $\psi_{\xi\eta}$, p_0, T_0) evaluated at the interface and for the deformation $h_1(x)$ by itself. Results show that the algorithm maintains approximately second-order accuracy.

Test 4 has been added in order to illustrate the effects of

TABLE II

Results of Grid Convergence Tests of the Algorithm Solving (Small) Deformation Equation (Section III.F)

Test	ψ_η	$\psi_{\xi\eta}$	p_0	T_0	h_1 fixed contact points	h_1 fixed contact angles
1 ($\mathrm{Bi} = 10^4$)	1.85	1.84	1.70	1.99	1.73	1.94
2 ($\mathrm{Bi} = 10^4$)	1.77	2.10	1.80	1.83	2.80	2.50
3 ($\mathrm{Bi} = 10^4$)	1.83	1.73	2.14	1.96	1.93	1.71
4 ($\mathrm{Bi} = 1$)	1.53	2.72	0.48	1.86	2.23	0.71

Note. Displayed results are for $T_{gx} = (0.5 - x)^2\,(0.5 + x)^2$, $\mathrm{Re} = \mathrm{Ma} = 30$, $L = 1$.

singularity in the temperature field at the contact points. It is a repetition of test 1 with Bi = 1 which leads to a rather benign singularity. Resuls show that the interface with moving contact points is strongly affected by inaccuracies in the representation of field quantities at the corners. A complete loss of accuracy in the case of strong singularities is possible.

The case of an initially flat interface, $h_0(x) = 1$, provides an opportunity for another test. Equation (15) reduces to the form

$$h_{1\xi\xi} = -W(\xi) - K, \qquad W(\xi) = p_0 + 2\psi_{\xi\eta} \tag{20a}$$

whose solution, corresponding to the fixed contact point conditions, is

$$h_1(\xi) = -\int_{-1/2L}^{\xi}\int_{-1/2L}^{\xi} W\,d\xi\,d\xi + 1/2K(L^2/4 - \xi^2) + (\xi/L + 1/2)\int_{-1/2L}^{1/2L}\int_{-1/2L}^{\xi} W\,d\xi\,d\xi, \tag{20b}$$

where

$$K = 24L^{-3}\int_{-1/2L}^{1/2L}\int_{-1/2L}^{\xi}\int_{-1/2L}^{\xi} W\,d\xi\,d\xi\,d\xi - 12L^{-2}\int_{-1/2L}^{1/2L}\int_{-1/2L}^{\xi} W\,d\xi\,d\xi.$$

Solution in the fixed contact angles case is

$$h_1(\xi) = -\int_{-1/2L}^{\xi}\int_{-1/2L}^{\xi} W\,d\xi\,d\xi + (\xi^2/2L + \xi/2 - L/24)\int_{-1/2L}^{1/2L} W\,d\xi + L^{-1}\int_{-1/2L}^{1/2L}\int_{-1/2L}^{\xi}\int_{-1/2L}^{\xi} W\,d\xi\,d\xi\,d\xi. \tag{20c}$$

The above integrals were evaluated by repetitive use of the trapezoidal rule. Calculations for $\Delta\xi = \Delta\eta = \frac{1}{80}$, $\mathrm{Re} = \mathrm{Ma} = 30$, $\mathrm{Bi} = 1$, $L = 1$, $T_{gx} = (0.5 - x)^2\ (0.5 + x)^2$, show the maximum difference between deformations evaluated using both methods to be $O(10^{-7})$ in the fixed contact points case and $O(10^{-5})$ in the fixed contact angles case.

The final test involves comparison with the asymptotic solution given in Ref. [7], which is valid for elongated cavities, an initially flat interface, $\mathrm{Re} = \mathrm{Ma} = 0$, $\mathrm{Bi} = \infty$, linear temperature distribution at the interface and a capillary number sufficiently small so that $C = O(A^4)$, where $A \ll 1$ is the cavity aspect ratio (A = height/length). The solution was constructed formally in the limit $A \to 0$. Results displayed in Fig. 4 are for the fixed contact points case and were obtained using the present algorithms for $L = 5$ ($A = 0.2$), $C = 0.024$, and $\Delta\xi = \Delta\eta = \frac{1}{20}$. They match

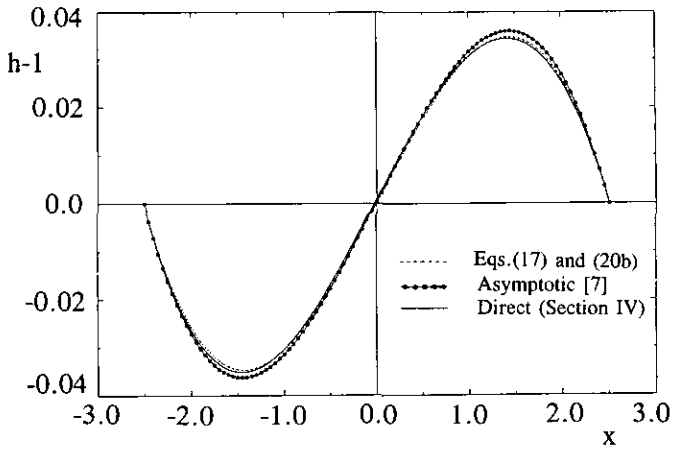

FIG. 4. Interface deformation $h_1(x)$ for fixed contact points case and initially flat interface ($D_L = D_R = 1$, $\mathrm{Re} = \mathrm{Ma} = 0$, $\mathrm{Bi} = \infty$, $T_{gx} = -1$, $L = 5$, $C = 0.024$).

the asymptotic results of Ref. [7] with the expected accuracy. For the fixed angles case, the solution given in Ref. [7] assumes that $h_{1x}(-\frac{1}{2}L) = -h_{1x}(\frac{1}{2}L) = A$. Calculations were carried out for $C = 0.008$, $L = 5$ ($A = 0.2$), and $\Delta\xi = \Delta\eta = \frac{1}{20}$. The results displayed in Fig. 5 again demonstrate agreement with the asymptotic solution.

G. *Limits of the Applicability of the Domain Perturbation Solution*

The domain perturbation solution was constructed as a first term in the asymptotic expansion in the powers of capillary number C for $C \to 0$ (Eq. (5)). Figure 6 presents the comparison between this solution and the solution of the complete moving boundary problem obtained using the algorithm described in Section IV. The results demonstrate that the error of the domain perturbation solution increases

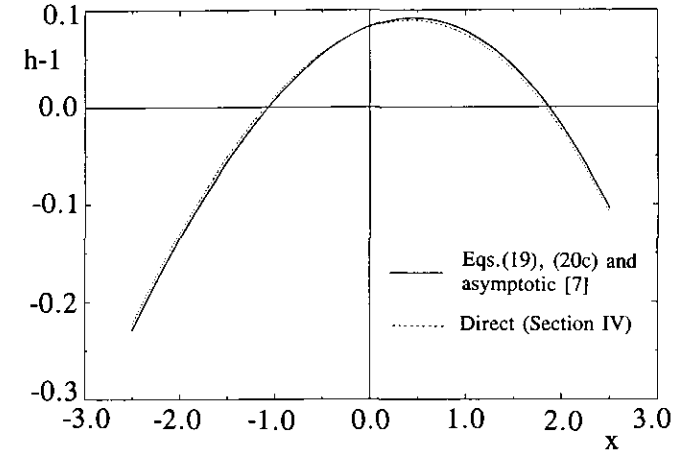

FIG. 5. Interface deformation $h_1(x)$ for fixed contact angles case and initially flat interface ($\tan\theta_L = 0.2$, $\tan\theta_R = -0.2$, $\mathrm{Re} = \mathrm{Ma} = 0$, $\mathrm{Bi} = \infty$, $T_{gx} = -1$, $L = 5$, $C = 0.008$).

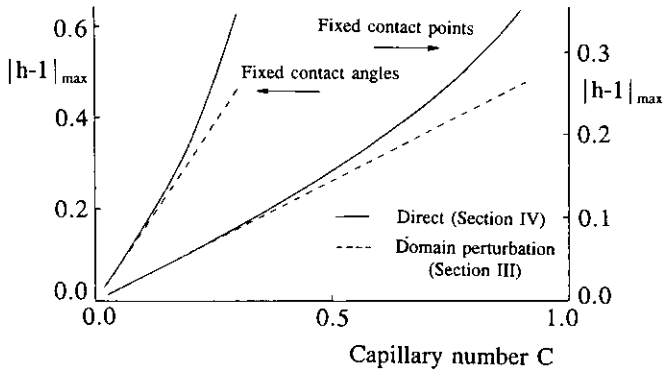

FIG. 6. Comparison between direct and domain perturbation solutions. $\mathrm{Re} = \mathrm{Ma} = 30$, $\mathrm{Bi} = 1$, $L = 5$, $T_{gx} = -1$, interface initially flat: Case A, fixed contact points ($D_L = D_R = 1$); Case B, fixed contact angles ($\theta_L = \theta_R = 0$).

proportionally to C^2, thus confirming the regular character of the expansions (5). The upper bound on the capillary number for which the domain perturbation method produces the solution within a desired accuracy may be estimated from diagrams given in Fig. 6.

IV. LARGE DEFORMATION SOLUTION

A. *The Algorithm*

When the final shape of the interface cannot be estimated accurately, the complete moving boundary problem (1)–(4) has to be solved directly. The problem is highly nonlinear (i) due to the presence of nonlinearities in the field equations (1), (ii) due to the unknown location of the interfacial boundary conditions, and (iii) due to the nonlinear character of these conditions by itself.

The algorithm developed here is based on Picard-type iteration on the shape of the interface. An initial approximation of the shape of the interface is made, then the field equations are solved with the assumed (known) location of the interface, and finally, the normal stress boundary condition is used to test whether the initial approximation of the interface was accurate. This procedure is repeated until convergence is reached. The logic of this algorithm is similar to the domain perturbation solution (Section III) and the only difference is in the treatment of the normal stress boundary condition.

B. *The Deformation Equation*

Normal stress boundary condition (2e) is re-written as

$$p - 2(1+h_\xi^2)^{-1} \times [-(1+h_\xi^2)\, h^{-1}\psi_{\xi\eta} + h_\xi h^{-2}(h_\xi^2 - h_{\xi\xi}h + 1)\psi_\eta] + C^{-1}h_{\xi\xi}(1-CT)(1+h_\xi^2)^{-3/2} = 0. \tag{21}$$

The pressure and shape of the interface are represented as

$$p = C^{-1}p_s + p_0 + K \tag{22a}$$

$$h = h_0 + h_1 \tag{22b}$$

$$p_s = -h_{0\xi\xi}(1+h_{0\xi}^2)^{-3/2}, \tag{22c}$$

where h_0 denotes the known shape of the isothermal interface corresponding to the known volume of the liquid (3), p_s stands for the known pressure of the isothermal liquid, h_1 denotes change of the shape of the interface due to nonisothermal effects, p_0 denotes the pressure associated with the thermocapillary convection and determined numerically from the solution of the field equations (Section III.F), and K stands for an arbitrary constant that can be present in the pressure field. Pressure p_0 satisfies the normalization condition $p_0(0, 1) = 0$. Equation (21) can be written for any grid point along the interface in the form

$$F_i(\hat{h}_i, \hat{h}_{\xi i}, \hat{h}_{\xi\xi i}, K) = 0, \tag{23}$$

where $\hat{h}_i$, $\hat{h}_{\xi i}$, $\hat{h}_{\xi\xi i}$, $i = 1, \ldots, N$, denote values of h_1, $h_{1\xi}$, $h_{1\xi\xi}$ at the grid points with $i = 1$ corresponding to the left contact point, and all the remaining quantities being known. Derivatives in (23) are approximated using standard central difference approximations leading to an equation in the form

$$F_i(\hat{h}_{i-1}, \hat{h}_i, \hat{h}_{i+1}, K) = 0 \tag{24}$$

which is then linearized using the Newton–Raphson procedure,

$$\begin{aligned} F_i(\hat{h}_{i-1}^{(k+1)}, \hat{h}_i^{(k+1)}, \hat{h}_{i+1}^{(k+1)}, K^{(k+1)}) &= F_i(\hat{h}_{i-1}^{(k)}, \hat{h}_i^{(k)}, \hat{h}_{i+1}^{(k)}, K^{(k)}) + \frac{\partial F_i}{\partial \hat{h}_{i-1}}(\hat{h}_{i-1}^{(k+1)} - \hat{h}_{i-1}^{(k)}) \\ &+ \frac{\partial F_i}{\partial \hat{h}_i}(\hat{h}_i^{(k+1)} - \hat{h}_i^{(k)}) + \frac{\partial F}{\partial \hat{h}_{i+1}}(\hat{h}_{i+1}^{(k+1)} - \hat{h}_{i+1}^{(k)}) \\ &+ (K^{(k+1)} - K^{(k)}) = 0. \end{aligned} \tag{25}$$

In the above, superscripts denote iteration count and derivatives are evaluated analytically at $\hat{h}_{i-1}^{(k)}$, $\hat{h}_i^{(k)}$, $\hat{h}_{i+1}^{(k)}$. Now Eq. (25) can be rewritten as

$$A_i\hat{h}_{i-1}^{(k+1)} + B_i\hat{h}_i^{(k+1)} + C_i\hat{h}_{i+1}^{(k+1)} + K^{(k+1)} = M_i^{(k)}, \tag{26}$$

where

$$M_i^{(k)} = \frac{\partial F_i}{\partial \hat{h}_{i-1}}\hat{h}_{i-1}^{(k)} + \frac{\partial F_i}{\partial \hat{h}_i}\hat{h}_i^{(k)} + \frac{\partial F_i}{\partial \hat{h}_{i+1}}\hat{h}_{i+1}^{(k)} + K^{(k)} - F_i^{(k)},$$

and $\hat{h}_{i-1}^{(k)}$, $\hat{h}_i^{(k)}$, $\hat{h}_{i+1}^{(k)}$ are known. Such an equation can be

written for each grid point along the interface. The above system of linear algebraic equations is closed by using volume constraint (3) and contact conditions (4).

Equation (3) takes the form

$$\int_{-1/2L}^{1/2L} h_1 \, d\xi = 0 \tag{25}$$

and is discretized using the trapezoidal rule. The matrix of coefficients for the complete system has the same structure as given by (17) for the fixed contact points case and by (19) for the fixed contact angles case. These systems can be solved directly using algorithms described in Appendices A and B.

The procedure described above for solution of the deformation equations has a quadratic rate of convergence. In all the numerical tests, three to four iterations were sufficient to reduce the error to the machine accuracy level.

C. *Numerical Tests*

All the discretization formulas used in the direct algorithm are formally of second-order accuracy. The actual performance of the algorithm was determined by carrying out solutions on the grids $\Delta\xi = \Delta\eta = \Delta = \frac{1}{20}, \frac{1}{40}, \frac{1}{80}$ and observing the tendency of the results as Δ was decreased. The effective accuracy was determined on the basis of Eq. (14). Results shown in Table III demonstrate that the algorithm delivers an accuracy that is closed to the second-order. The maximum interface deformation in these tests was about 20%.

As a second test, calculations were carried out for cases that are described either by the domain perturbation solution or by other asymptotic methods. Results displayed in Figs. 4–6 demonstrate that the direct algorithm accurately reproduces results obtained by other meethods.

The efficiency of the algorithm strongly depends on the particular values of the parameters present in the problem, like Re, Ma, and C. The most efficient solution was obtained by carrying out one iteration on the flow field, followed by one iteration of the interface. In all cases strong underrelaxation (0.01–0.1) was used when adjusting the shape of the interface. This underrelaxation increased with an increasing value of C. Field equations were treated as described in Section III.E. The iterations were carried out until all the convergence criteria for the field quantities (Section III.C) and similar criteria for the deformation equation (21) were satisfied.

TABLE III

Results of Grid Convergence Tests of the Direct Algorithm (Section IV.C)

	ψ	ω	T	p	h_1
Fixed contact points ($D_L = D_R = 1$, $C = 0.075$)	1.58	1.58	1.69	1.56	1.61
Fixed contact angles ($\theta_L = \theta_R = 0$, $C = 0.02$)	1.70	1.76	1.68	1.49	1.54

Note. Displayed results are for $T_{gx} = (1.5 - x)^2 \quad (1.5 + x)^2$, $\mathrm{Re} = \mathrm{Ma} = 20$, $\mathrm{Bi} = 10^4$, $L = 3$, initially flat interface.

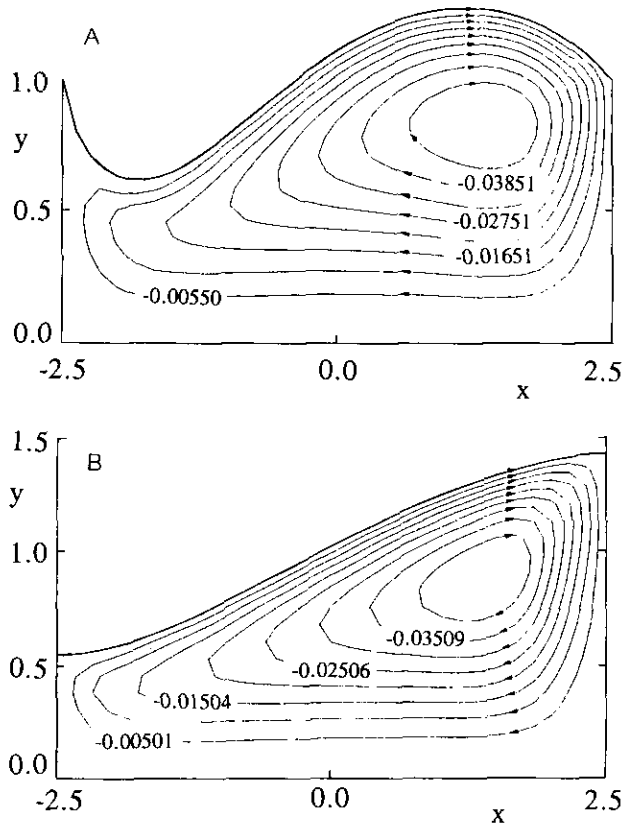

FIG. 7. Flow patterns in the large deformation case. $\mathrm{Re} = \mathrm{Ma} = 30$, $\mathrm{Bi} = 1$, $L = 5$, $T_{gx} = -1$, interface initially flat: Case A, fixed contact points case $D_L = D_R = 1$, $C = 0.2$; Case B, fixed contact angles case $\theta_L = \theta_R = 0$, $C = 0.05$.

The effect of the type of contact conditions on the response of the interface is illustrated in Figs. 7A–B. In both cases the interface is subject to the same external temperature field. The resulting shape of the interface and the topology of the flow field are qualitatively different. One may note that a much larger deformation is obtained by allowing the contact points to move (i.e., by applying fixed contact angle conditions) while keeping all other parameters without any change. This point is also vividly illustrated in Fig. 6. Because of that, a much stronger underrelaxation was required to obtain a convergent solution in the fixed contact angle case.

V. SUMMARY

An effective algorithm for analysis of the dynamics of nonisothermal capillary interfaces has been developed. The

algorithm solves the moving boundary problem for the Navier–Stokes and energy equations. Accurate modelling of the surface tension effects and the viscous stresses at the interface is assured by implementation of the coordinate transformation method. The unknown physical domain is mapped onto a rectangular computational domain, with the explicit form of the mapping function not being known. The field variables and the mapping function are determined simultaneously using Picard-type iteration on the normal stress boundary condition at the interface. The algorithm uses streamfunction–vorticity formulation for the flow variables. All the discretization formulas are second-order accurate. Numerous tests show that the algorithm delivers second-order accuracy even for very large interfacial distortions.

APPENDIX A

This appendix describes an algorithm for the direct solution of the matrix equation (17). The diagonal terms are eliminated leading to a solution in the form

$$\hat{h}_i = -H_i \hat{h}_{i+1} + G_i + E_i K, \tag{A1}$$

where

$$\begin{aligned} H_i &= C_i/(B_i - A_i H_{i-1}), \\ G_i &= (M_i - A_i G_{i-1})/(B_i - A_i H_{i-1}), \\ E_i &= (N_i - A_i E_{i-1})/(B_i - A_i H_{i-1}). \end{aligned} \tag{A2}$$

Coefficients H_i, G_i, E_i, are evaluated for $i = 1, ..., N-1$ by noting that $H_1 = 0$, $E_1 = 0$, $G_1 = \hat{h}_1$, $A_2 = 0$. The bottom row of the matrix is eliminated by writing a partial sum in the form

$$S_i = P_i \hat{h}_i + R_i + F_i K, \tag{A3}$$

where

$$\begin{aligned} &P_i = -P_{i-1} H_{i-1} + D_i, \qquad R_i = P_{i-1} G_{i-1} + R_{i-1}, \\ &F_i = P_{i-1} E_{i-1} + F_{i-1}. \end{aligned} \tag{A4}$$

These sums are evaluated for $i = 2, ..., N$ by noting that $S_2 = D_2 \hat{h}_2$, thus $P_2 = D_2$, $R_2 = 0$, and $F_2 = 0$; also, $D_N = 0$. Pressure constant K is evaluated from the total sum as

$$K = (W - P_N \hat{h}_N - R_N)/F_N. \tag{A5}$$

The complete solution procedure involves evaluation of H_i, G_i, E_i from (A2), followed by evaluation of P_i, R_i, F_i from (A4), calculation of K from (A5), and evaluation of $\hat{h}_i$ from (A1).

APPENDIX B

This appendix describes an algorithm for the direct solution of the matrix equation (19). Equation (A1) is used with H_i, G_i, E_i defined by (A2) for $i = 1, ..., N$, with $H_1 = (C_1 C_2 - B_2 G_1)/(B_1 C_2 - A_2 G_1)$, $G_1 = (M_1 C_2 - M_2 G_1)/(B_1 C_2 - A_2 G_1)$, and $E_1 = -N_2 G_1/(B_1 C_2 - A_2 G_1)$. Partial sums are defined by (A3) for $i = 1, ..., N$ with $P_1 = D_1$, $R_1 = 0$, $F_1 = 0$. Expression for the pressure constant assumes the form

$$K = \frac{(V - R_N) A^* + C^* P_N}{F_N A^* - P_N B^*} \tag{B1}$$

with

$$\begin{aligned} A^* &= -A_N A_{N-1} H_{N-1} + B_{N-1} G_N H_{N-1} \\ &\quad + B_N A_{N-1} - C_{N-1} G_N \\ B^* &= A_N A_{N-1} E_{N-1} - B_{N-1} G_N E_{N-1} + N_{N-1} G_N \\ C^* &= A_N A_{N-1} G_{N-1} - B_{N-1} G_N G_{N-1} \\ &\quad - M_N A_{N-1} + M_{N-1} G_N. \end{aligned}$$

Location of the right contact point is defined as

$$\hat{h}_N = \frac{(V - R_N) B^* + C^* F_N}{P_N B^* - A^* F_N}$$

and all the remaining points can be evaluated from the recursion relation (A1).

ACKNOWLEDGMENT

The authors would like to acknowledge support of this work provided by the NSERC of Canada.

REFERENCES

1. J. M. Floryan and H. Rasmussen, Numerical methods for viscous flows with moving boundaries, *Appl. Mech. Rev.* **42**, 323 (1989).
2. H. Shokoohi and H. G. Elrod, Numerical investigation of the disintegration of liquid jets, *J. Comput. Phys.* **71**, 324 (1987).
3. F. Shokoohi and H. G. Elrod, Algorithms for Eulerian treatment of jet breakup induced by surface tension, *J. Comput. Phys.* **89**, 483 (1990).
4. M. Strani and R. Piva, Surface tension driven flows in microgravity conditions, *Int. J. Numer. Methods Fluids* **2**, 367 (1982).
5. J. C. Chen, J. C. Sheu, and S. S. Jwu, Numerical computation of thermocapillary convection in a rectangular cavity, *Numer. Heat Transf.* **17**, 287 (1990).
6. A. Rybicki and J. M. Floryan, Thermocapillary effects in liquid bridges, *Phys. Fluids* **30**, 1956 (1987).
7. A. K. Sen and S. H. Davis, Steady thermocapillary flows in two-dimensional slots, *J. Fluid Mech.* **121**, 163 (1982).